POLISH MARITIME RESEARCH 2 (122) 2024 Vol. 31; pp. 67-76
10.2478/pomr-2024-0022

Experimental Validation of an FEM Model Based on Lifting Theory Applied to Propeller Design Software

Andrzej Grządziela [1]
Marek Kraskowski [2*]
Przemysław Król [2]
Bogdan Szturomski [1]
Radosław Kiciński [1]
[1] Polish Naval Academy, Gdynia, Poland
[2] Maritime Advanced Research Centre(CTO S.A.), Gdansk, Poland

* Corresponding author: *marek.kraskowski@cto.gda.pl (Marek Kraskowski)*

ABSTRACT

In the process of designing a marine propeller, hydroelasticity effects are neglected in most cases, due to the negligible influence of the blade's deformation on its hydrodynamic characteristics. However, there are cases where the impact of hydroelasticity is crucial, for example in the case of high skew-back propellers or heavy-loaded composite propellers. Furthermore, the importance of composite propellers is growing due to their wide range of application, for instance in naval ships and unmanned vehicles. Although structural models and two-way fluid-structure interactions are implemented in most commercial CFD solvers, their relevance to the design process is severely limited due to the high computational cost for a single iteration. An effective solution would therefore be to implement a two-way fluid-structure interaction model in the lifting surface software, which is commonly accepted as a design tool due to its relatively low computational time and its applicability to multi-criteria optimisation. This paper presents the results of hydrodynamic analyses of an elastic propeller carried out using in-house software based on the lifting surface flow model, and extended with the FEM model for the blade structure. The results are compared with experimental measurements and computational analyses with the commercial RANS solver STAR-CCM+.

Keywords: scale model tests, CFD, marine propeller, fluid-structure interaction

INTRODUCTION

The work presented in this paper was carried out within the framework of the NextProp project, and focused on the development of design tools for modelling low-noise naval propellers. The project represents a response to the growing popularity of composite materials in marine applications. Ships made of composite and polymer materials are already in use: the Polish Navy has project 207 minesweepers, the Royal Norwegian Navy has Skjøld project ships, and the Royal Swedish Navy operates on Visby-class corvettes made entirely of composites [1]. Another example application is the use of highly attenuating composite materials to reduce the acoustic signature of a submarine's propeller [2]. In this context, and to enable the introduction of composite solutions to shipbuilding, methods of designing and analysing flow for deformable propulsors need to be developed, as reported in [3–5]. Well-designed composite propellers offer the possibility of increased efficiency and reduced noise compared to metal propellers, due to the effect of passive adaptation of hydroelastic

blades [6]. However, the hydroelasticity of the propeller blades influences their hydrodynamic characteristics, which poses new challenges for the propeller designer, since most typical design tools model the propeller as a rigid body [1].

Computational tools offering fluid-structure interaction (FSI) analyses have reached a high level of maturity during the last decade [8]. In most cases, FSI analyses are based on a partitioned approach, where the fluid flow and the structure deformation are analysed by separate solvers and convergence between them is achieved in an iterative manner. This approach can be divided into one-way coupling and two-way coupling techniques [9]. There have also been attempts to carry out FSI analyses using a monolithic approach, in which the solutions for the fluid and solid domains in each time step are achieved by solving a single system of equations [10]. The finite element method (FEM) enables analysis of a composite material by direct modelling of its layers, taking into account the anisotropy of the materials [11]. Based on the results presented in the recent literature, it can be stated that accurate modelling of the operation of composite propellers with modern computational tools is possible with high accuracy, and can take into account all of the features of the composite material. However, a design tool is not necessarily expected to provide the highest possible accuracy; instead, it is required to capture trends correctly and to generate an optimum geometry within a reasonable time. For this reason, compromises are often necessary, resulting in simplifications of the computational model.

The work presented here focuses on extending an in-house propeller design software based on lifting surface theory with an FEM module, which allows us to correctly take into account the blade deflection. Validation is carried out based on experimental measurements and RANS CFD analyses, and focuses on a quantitative comparison of the blade tip deflection. Two cases are selected for analysis as part of the NextProp project: an asymmetric foil with high aspect ratio, and a SINTEF P1566 marine propeller. Good coincidence was observed between all hydrodynamic analysis methods, thus proving the applicability of the developed software to the elastic propeller design process.

DEVELOPMENT OF THE FEM MODULE FOR THE PROPELLER DESIGN SOFTWARE

To carry out propeller design, CTO SA uses in-house software based on the lifting surface model. This means that the propeller blade is modelled by "horseshoe vortices" distributed over a surface defined by the skeletal lines of the propeller blade profile (Fig. 1). The circulation for each vortex is computed by solving a system of equations that is formulated to meet the non-permeability boundary condition at the lifting surface. The blade thickness is modelled in a simplified way by distributing the point sources over the lifting surface.

Fig. 1. Modelling a foil with a lifting surface

Until now, the deflection of the propeller blade has never been considered during the propeller design process. The work presented here and carried out within the framework of the NextProp project involves extending the current in-house software with an FEM module to allow for coupling between the evaluation of the flow around the propeller blades and the assessment of the blade deformation. The developed module is expected to meet the following requirements:

- Two-way coupling is needed between the flow and the blade deformation, and the flow should be evaluated iteratively until convergence is reached;
- Shell elements should be used to enable the modelling of arbitrary blade shapes;
- The blade must be modelled with a single layer of elements, to reduce the computation time.

The structural elements used in the developed FEM module are eight-node shell elements with second-order polynomials used as shape functions [12–14].

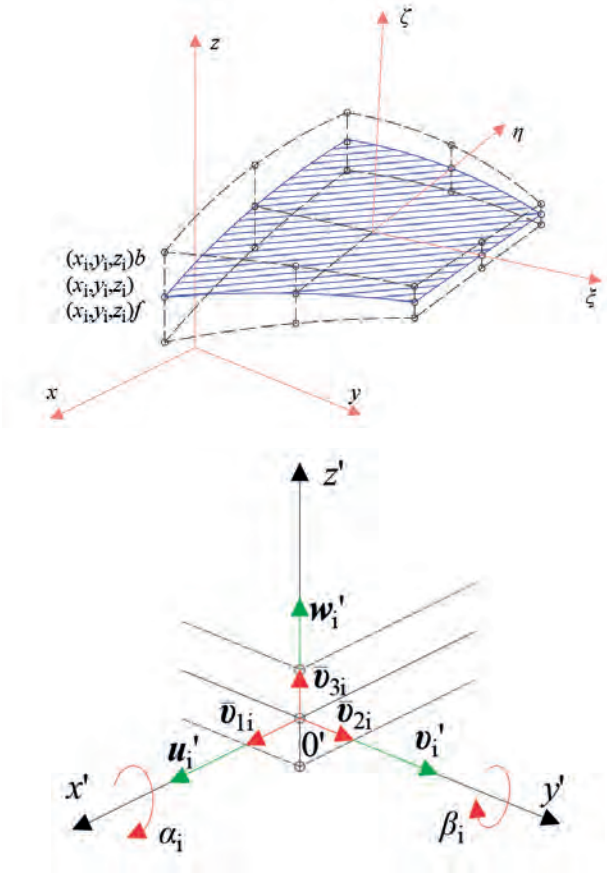

Fig. 2. Diagrams of the element type and nodal coordinate system

Modelling of the blade in this manner provides relatively high versatility at a moderate cost; however, its applicability is limited to isotropic materials. In addition, since the lifting surface is used to model the flow, this means that the software is dedicated to analyses of propeller loading conditions close to the maximum efficiency point, as the results for conditions close to bollard pull, under which strong separation occurs, are incorrect when the lifting surface is used.

The lifting surface mesh used for the propeller analyses reported in this paper is presented in Fig. 3.

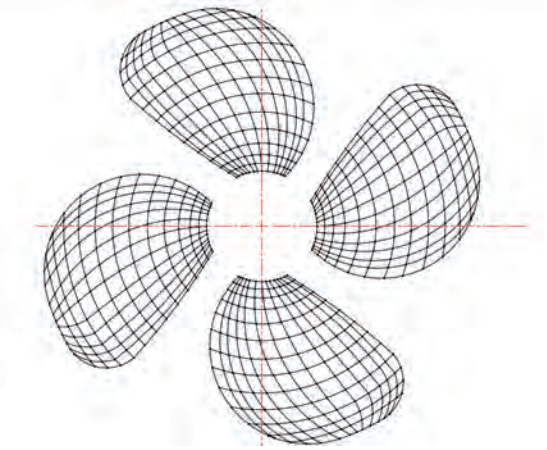

Fig. 3. Panel mesh used for the lifting surface analyses

VALIDATION CASES

Validation of the developed FEM module for the propeller design software was based on two cases, involving a foil and a marine propeller, both under uniform flow. Some general data for both objects are summarised below.

Foil case

The following dimensions characterise the foil used for validation:

- Chord length at the root: 160 mm;
- Chord length at the tip: 80 mm;
- Span: 400 mm;
- Profile thickness: 10.5% of the chord length.

The foil outline and profile are presented in Fig. 4.

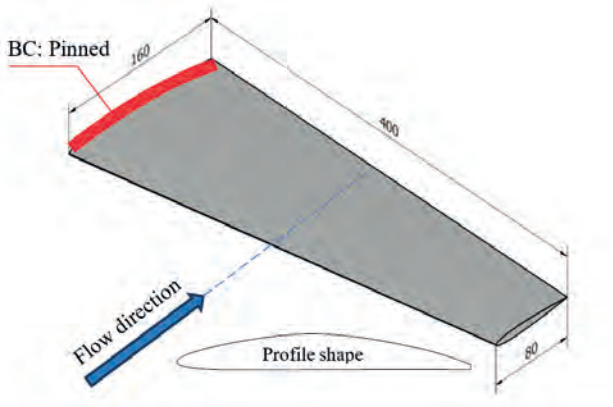

Fig. 4. Foil outline and profile

Three foil models were manufactured from different materials characterised by considerably different values for the stiffness:

- Steel: Young modulus 210 GPa (rigid steel foil, RSF);
- Chopped strand mat (CSM): 7.433 GPa (flexible isotropic composite foil, FICF);
- Polyacetal (POM): 3.683 GPa (POM).

All of the materials used to manufacture the foil models can be considered isotropic.

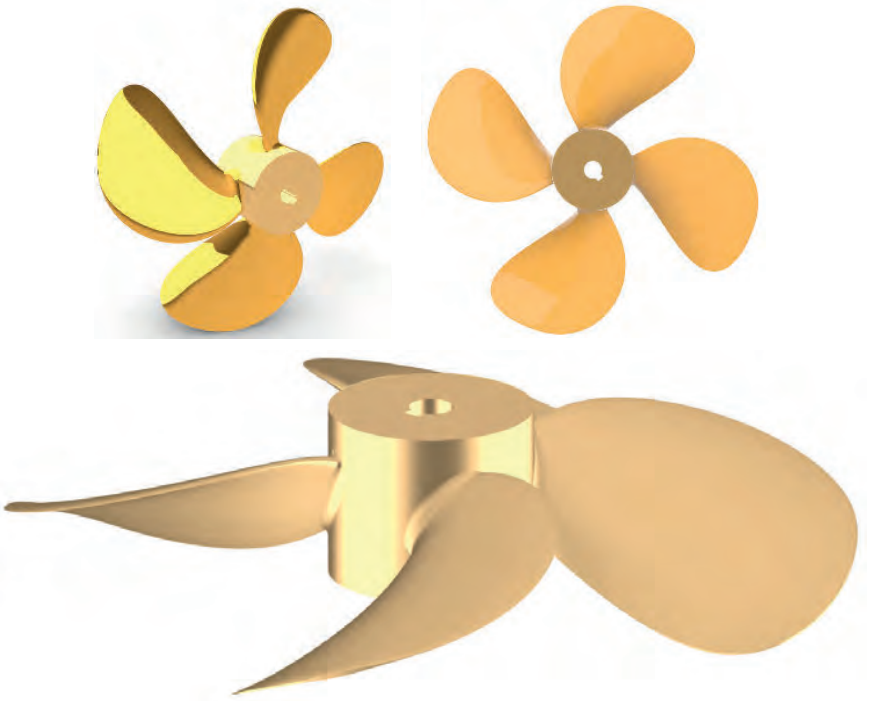

Fig. 5. Propeller outline and 3D visualisation

Propeller case

The main features of the propeller used for validation are as follows:

- Outer diameter D: 250 mm;
- Relative hub diameter d/D: 0.24;
- Design pitch ratio P/D: 1.1;
- Expanded area ratio: 0.6.

An outline of the propeller and a 3D visualisation are presented in Fig. 5.

Two propeller models were manufactured from different materials characterised by considerably different values for the stiffness:

- Bronze: Young modulus 95.8 GPa;
- Polyacetal (POM): 3.133 GPa.

Both of the materials used to manufacture the propeller models can be considered isotropic. The difference in the POM stiffness between the foil and propeller results from the differences in manufacturing technology.

EXPERIMENTAL SETUP AND TEST MATRICES

All the experiments used as a reference for validation of the computational analyses were carried out in the cavitation tunnel at the Maritime Advanced Research Centre CTO SA. The length of the tunnel's measurement chamber is 3080 mm, and the cross-section is square, with dimensions of 800 × 800 mm. The experiments with the foil included measurements of the hydrodynamic characteristics, detailed flow field quantification, and measurements of the tip deflection. For the flow field measurements and tip deflection measurements, a separate mounting was used to prevent the elasticity of the dynamometer influencing the result. The measurement chamber and the location of the foil inside it are shown in Fig. 6.

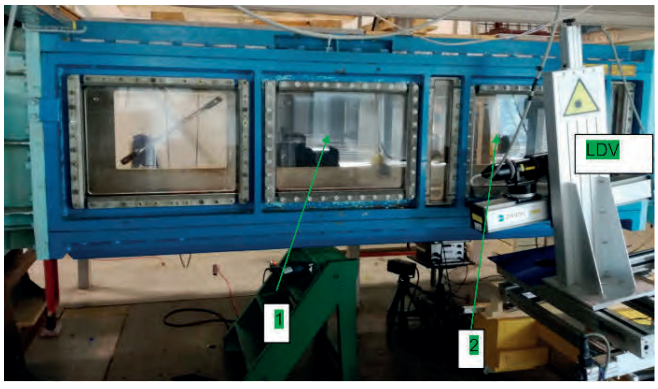

Fig. 6. Measurement chamber of the cavitation tunnel. Location 1 – measurements of the flow field and tip deflection; Location 2 – measurements of forces and moment (LDV – Laser doppler velocimeter).

The foil is shown inside the measurement chamber in Fig. 7.

Fig. 7. Foil inside the tunnel – Location 2.

The test matrix included all combinations of the following values of the flow speed and angle of attack:

- Flow speed: 2, 3, 4 and 6 m/s;
- Angle of attack: –1°, 0°, 1°, 3° and 5°.

The measurements with the propeller were carried out using dedicated streamlined housing for the dynamometer, with the propeller mounted upstream.

The experiments included measurements of the generated noise and blade tip deflection for the specified loading conditions. The propeller thrust coefficient K_T defines the loading conditions at a given revolution rate. Four revolution rates were considered: 7, 9, 11 and 20 RPS. The values of the thrust coefficient were: 0.2, 0.4 and 0.5. At 20 RPS, the only value of K_T considered was 0.2, since higher values were not achievable due to the dynamometer's measurement range and the model's strength. Using a high-speed camera, the blade tip deflection was measured by comparing digital images taken at zero thrust and at a specified value of thrust. An example of two pictures of loaded and unloaded propellers is presented in Fig. 8. In the case shown here, it was not possible to detect any differences in the generated noise, either for different propeller loading conditions or for different blade materials.

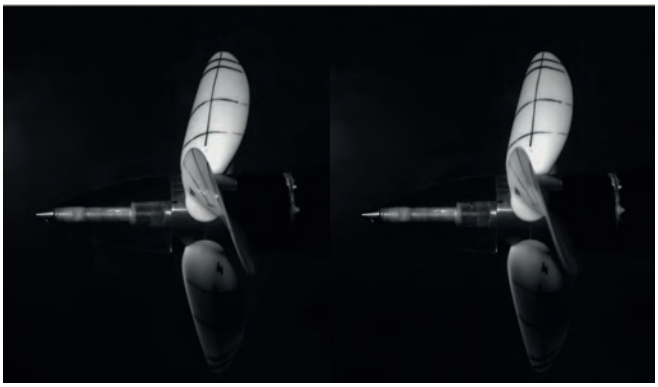

Fig. 8. Images of the elastic propeller in the cavitation tunnel for zero thrust (left) and highest thrust (right)

REFERENCE RANS CFD ANALYSES

As an additional verification of the developed FEM model and also of the experiment itself, CFD computations involving two-way fluid-structure interaction were carried out for the cases of both the foil and the propeller. The well-known and widely verified commercial software STAR-CCM+ was used; this is based on the Reynolds averaged Navier-Stokes (RANS) flow model, and enables FSI analyses based on the partitioned approach with two-way coupling.

The computations for the foil were carried out in a rectangular domain, with a cross-section corresponding to the actual dimensions of the CTO cavitation tunnel, i.e. 800 × 800 mm. Each case was analysed considering the fluid-structure interaction; in other words, the flexibility of the foil was modelled directly for the steel foil. The number of mesh cells was 9.3 million for the fluid domain (hexahedral elements) and 250,000 for the solid domain (eight-node solid elements). Sample visualisations of the mesh are shown in Figs. 9 and 10.

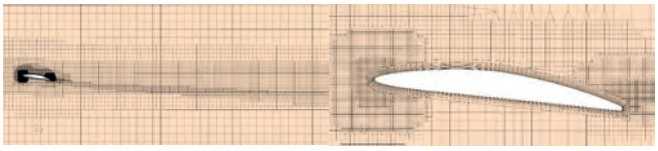

Fig. 9. Computational mesh for RANS-CFD: fluid domain

Sample visualisations of the results are given in Fig. 11.

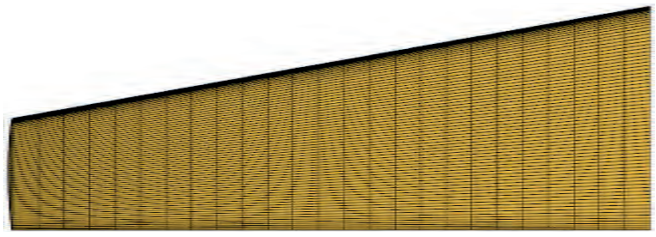

Fig. 10. Computational mesh for RANS-CFD: solid domain

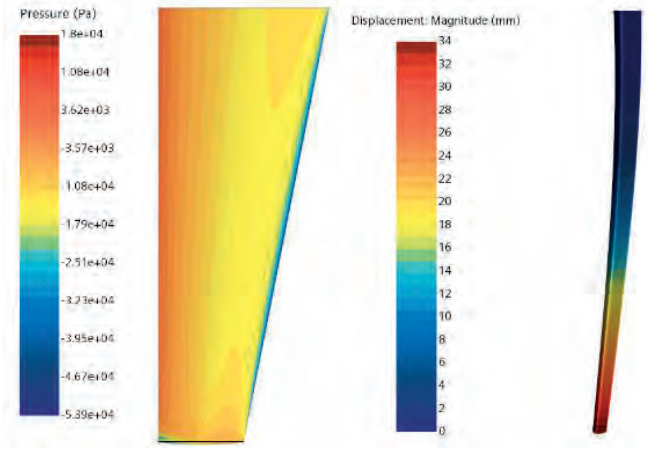

Fig. 11. Sample visualisations of the results: pressure distribution (left) and foil deformation (right)

The following solver settings were applied:

- Coupled flow;
- Steady state;
- Turbulence model: Realisable k-epsilon.

The properties of the water were as follows:

- Density: 997.561 kg/m^3;
- Kinematic viscosity: 8.91e-07 m^2/s.

For each case, the computations were started with a rigid foil; after stabilisation of the forces, the FSI analysis was started. Convergence for a particular case is presented in Fig. 12. After 300 iterations, deformation of the foil was enabled.

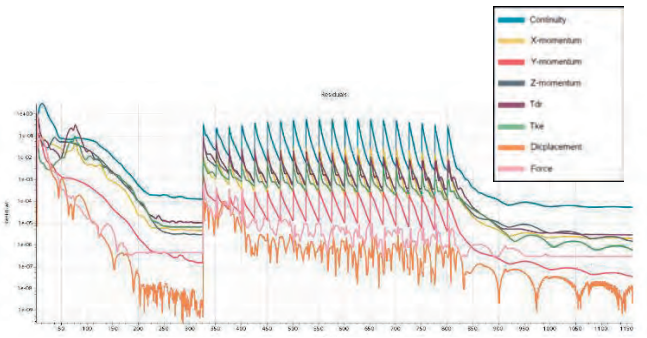

Fig. 12. Convergence for the foil case: residuals

The computations for the propeller were carried out based on unrestricted flow conditions in a sector of a cylindrical domain covering a single blade, with periodic boundary conditions (Fig. 13).

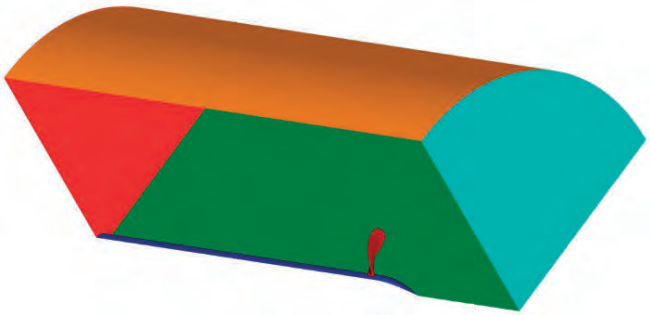

Fig. 13. Computational domain for RANS-CFD: general view

The fluid domain was composed of 1,864,000 polyhedral cells. For the solid body, due to problems with generating a hexahedral mesh for the blade without simplification of the geometry, a tetrahedral mesh was used. The solid domain was composed of 138,700 cells, and the boundary condition for evaluation of the blade deformation was applied to the intersection of the blade surface with the cylindrical hub surface. All degrees of freedom were constrained.

The influence of the mesh density on the results for the propeller case, which was the crucial one in this study, was verified by comparing the thrust and torque for six different meshes. The STAR-CCM+ solver enables the user to change

the size of the mesh elements and the density by changing just one parameter, the base size, on which all the remaining mesh parameters depend. The mesh parameters and the resulting thrust and torque for single blade for the selected flow conditions (11 rpm, KT = 0.4) are presented in Table 1 and Fig. 14.

Tab. 1. Results of the mesh density study

Mesh no.	Base size [m]	Cells [1*10^6]	Thrust [N]	Torque [Nm]
1	0.040	0.126	24.054	1.238
2	0.030	0.190	23.388	1.211
3	0.020	0.375	23.567	1.220
4	0.015	0.710	23.440	1.217
5	**0.010**	**1.864**	**23.433**	**1.216**
6	0.075	4.364	23.442	1.213

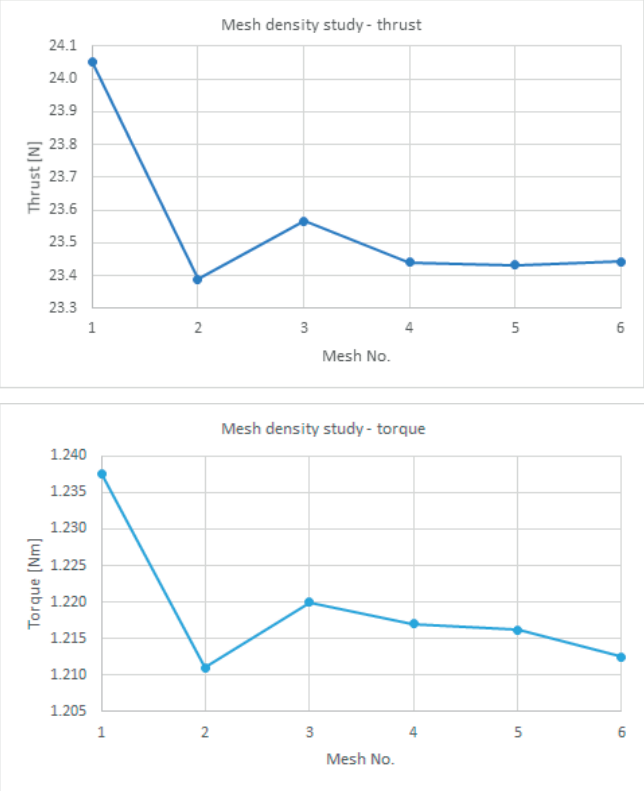

Fig. 14. Results of the mesh density study

It can be seen that for the default mesh No. 5, there is no further reduction in the numerical error by further increasing the mesh density. For the torque, no clear convergence was obtained, but a further increase in the mesh size would have resulted in an unacceptable computational time. Moreover, this is the thrust that is crucial from the point of view of blade deflection.

The influence of the turbulence model was verified by comparing the resulting thrust and torque for the default mesh and for two turbulence models, based on realisable k-epsilon and SST k-omega. The difference in both cases was below 1%. The solver's default realisable k-epsilon model was finally selected for all cases.

Visualisations of the mesh at the surface of the blade for the fluid and solid domains are presented in Fig. 15.

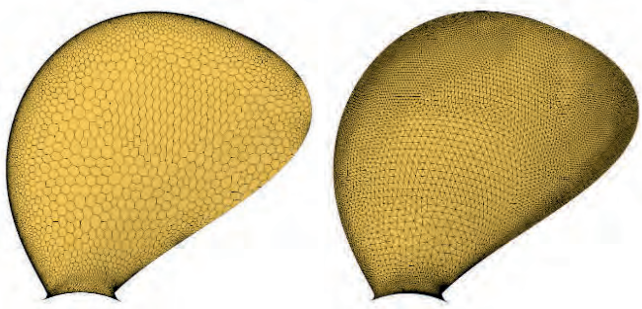

Fig. 15. Surface mesh on the blade: fluid domain (left) and solid domain (right)

The solver settings for the propeller were the same as for the foil. Sample visualisations of the results are presented in Fig. 16, where the differences in the pressure distribution for the lowest and highest thrust coefficient K_T are shown. To enable a comparison of the considerably different loading conditions, the pressure is represented in the form of a non-dimensional coefficient, defined as:

$$C_P = \frac{p}{0.5\rho \cdot (2\pi n \cdot 0.7R)^2}$$

where:

- p is the pressure in Pa;
- ρ is the water density in kg/m^3;
- n is the revolution rate in RPS;
- R is the propeller radius in m.

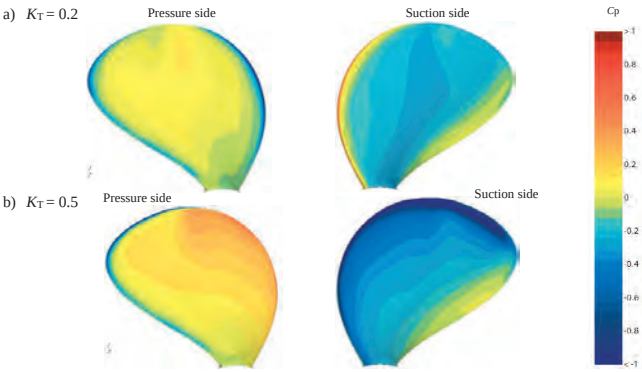

Fig. 16. Sample visualisations of CFD results for the propeller

RESULTS

The values for the hydrodynamic loads and tip deformation obtained from measurements, the RANS CFD simulations, and the developed in-house software are compared in this section. The results for the foil case include the drag force, lift force, twisting moment and tip deflection at the trailing edge. The experiment revealed minor differences between the lift, drag and moment for models with different stiffnesses. The RANS CFD computations revealed hardly any differences, so the differences observed in the experiments probably resulted from their uncertainties. The hydrodynamic forces were therefore compared for a single case, involving a steel foil and a speed of 4 m/s. For a velocity of 6 m/s, strong aeration at the foil root was observed, and the results were considered inconclusive.

The resulting lift force values are summarised in Fig. 17 and Table 2. In general, an underestimate of the lift at the lifting surface is observed.

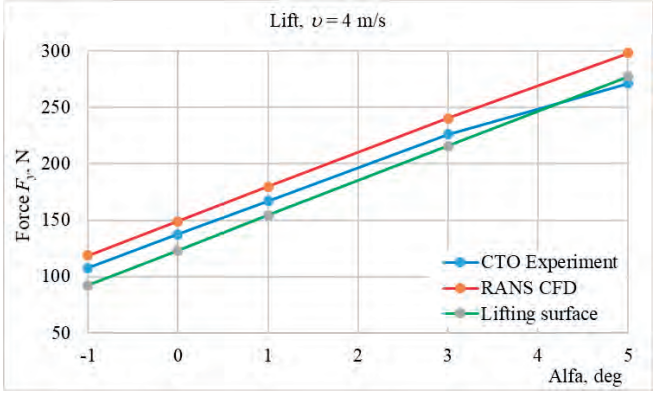

Fig. 17. Comparison of measured and computed values for the lift of the foil

Tab. 2. Comparison of measured and computed values of the moment of the foil

	Lift [N]				Difference [%]	
α [deg]	Exp.	RANS	Lift. surf.	Std. dev [N]	Exp/ RANS	Exp/ LIFT
–1	107.6	118.8	92.4	13.2	10.4	-14.2
0	137.6	149.1	122.8	13.2	8.4	-10.8
1	167.1	179.6	154.4	12.6	7.5	-7.6
3	226.3	240.3	215.8	12.3	6.2	-4.6
5	271.6	298.4	277.6	14.1	9.9	2.2

The resulting drag force values are shown in Fig. 18 and in Table 3. A different character of the drag curve evaluated based on the lifting surface is visible, as the evaluation of drag with this method is, by definition, less accurate.

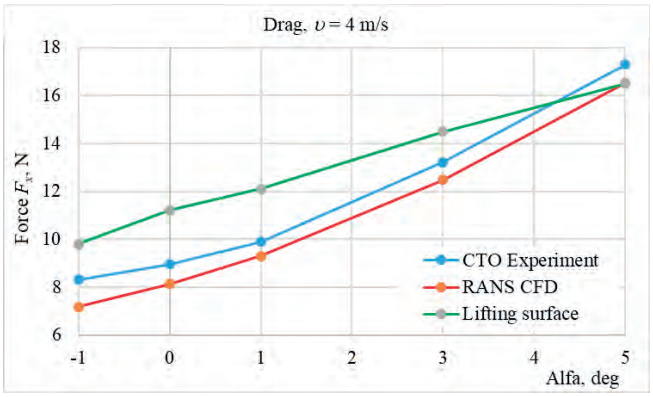

Fig. 18. Comparison of measured and computed values of drag for the foil

Tab. 3. Comparison of measured and computed drag for the foil

	Drag [N]				Difference [%]	
α [deg]	Exp.	RANS	Lift. surf.	Std.dev [N]	Exp/ RANS	Exp/ LIFT
–1	8.31	7.18	9.80	1.3	–13.6	17.9
0	8.96	8.13	11.20	1.6	–9.3	25.0
1	9.89	9.30	12.10	1.5	–6.0	22.3
3	13.21	12.49	14.50	1.0	–5.5	9.8
5	17.30	16.52	16.50	0.5	–4.5	–4.6

The resulting twisting moments are summarised in Fig. 19 and Table 4. The largest discrepancies are observed between the experimental and computational results, as well as between the computational models. One conclusion is that in the case considered here, the computed value of the twisting moment is extremely sensitive to the accuracy of evaluation of the pressure distribution on the foil surface, especially when the absolute values of the twisting moment are relatively small (balanced foil). On the other hand, experimental results are susceptible to the accuracy of mounting of the model.

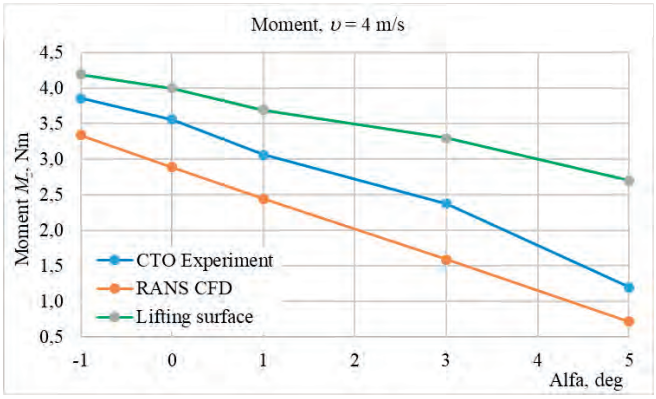

Fig. 19. Comparison of measured and computed values of the moment for the foil

Tab. 4. Comparison of measured and computed values of the moment for the foil

	Moment [Nm]				Difference [%]	
α [deg]	Exp.	RANS	Lift. surf.	Std. dev [Nm]	Exp/ RANS	Exp/ LIFT
–1	3.86	3.34	4.20	0.4	–13.4	8.8
0	3.56	2.89	4.00	0.6	–18.8	12.4
1	3.07	2.45	3.70	0.6	–20.3	20.5
3	2.38	1.59	3.30	0.9	–33.2	38.7
5	1.20	0.72	2.70	1.0	–40.3	125.0

The tip deflection values for the foil were compared at the highest speed of 6 m/s, to minimise the uncertainty. For steel foil, tip deflections of up to 1 mm were measured. The results of the experiments and computations for flexible foils are presented in Figures 20 and 21 and in Tables 4 and 5. The discrepancies for polyacetal foil are considerable; however, the agreement is generally still reasonably good, and it can be seen that the computations using lifting surface remain stable for values of the tip deflections as large as 60 mm, i.e. 15% of the foil span.

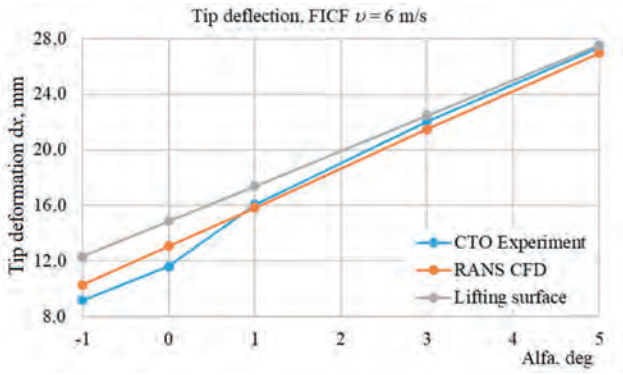

Fig. 20 Comparison of measured and computed tip deflection – flexible isotropic composite foil

Tab. 4. Comparison of measured and computed tip deflection – flexible isotropic composite foil

	Tip deflection [mm]				Difference [%]	
Alfa [deg]	Exp.	RANS	Lift. surf.	Std.dev [N]	Exp/ RANS	Exp/ LIFT
–1	9.18	10.30	12.33	1.6	12.2	34.3
0	11.61	13.07	14.86	1.6	12.5	28.0
1	16.06	15.83	17.39	0.8	–1.5	8.3
3	22.01	21.50	22.46	0.5	–2.4	2.0
5	27.35	26.97	27.52	0.3	–1.4	0.6

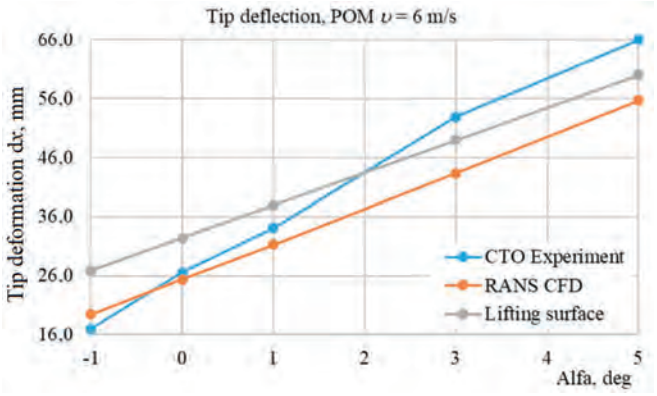

Fig. 21. Comparison of measured and computed values of tip deflection for a polyacetal foil

Tab. 5. Comparison of measured and computed tip deflection for a polyacetal foil

	Tip deflection [mm]				Difference [%]	
α [deg]	Exp.	RANS	Lift. surf.	Std. dev [N]	Exp/ RANS	Exp/ LIFT
–1	17.02	19.48	26.88	5.1	14.5	57.9
0	26.56	25.35	32.39	3.8	–4.6	21.9
1	34.16	31.26	37.91	3.3	–8.5	11.0
3	52.90	43.34	48.96	4.8	–18.1	–7.5
5	66.00	55.65	59.99	5.2	–15.7	–9.1

For the propeller case, our comparison of the results focuses on the deflection of the blade tip. The computations carried out using a lifting surface are, by definition, less accurate for low advance ratio values, so the analyses were tuned by making minor adjustments to the blade pitch to match the experimental values of the thrust coefficient K_T more closely. The blade tip deflection values are presented as a function of each method's actual thrust coefficient value. The results are presented for each revolution rate separately in Figures 22–24. A quantitative comparison was not possible in this case due to the different values of the thrust coefficient obtained for each scenario. At 20 RPS, only the deflection for the lowest thrust coefficient ($K_T = 0.2$) was obtained, so a graph is omitted from this paper.

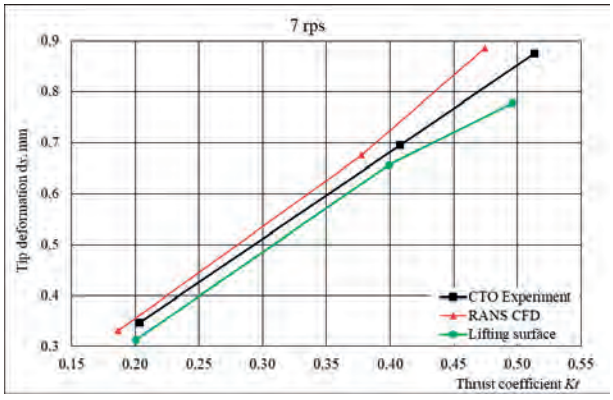

Fig. 22. Computed values of the tip deflection compared with experimental data, at 7 RPS

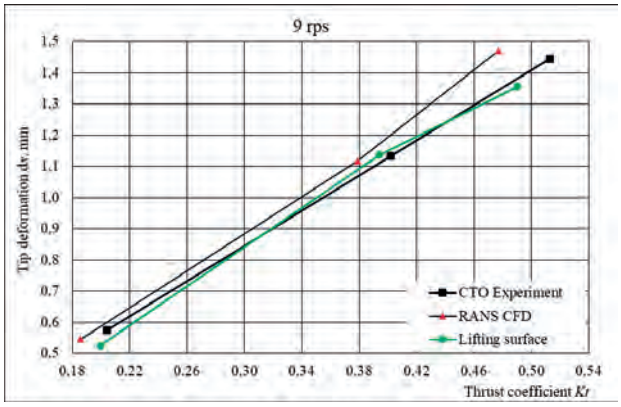

Fig. 23. Computed values of the tip deflection compared with experimental data, at 9 RPS

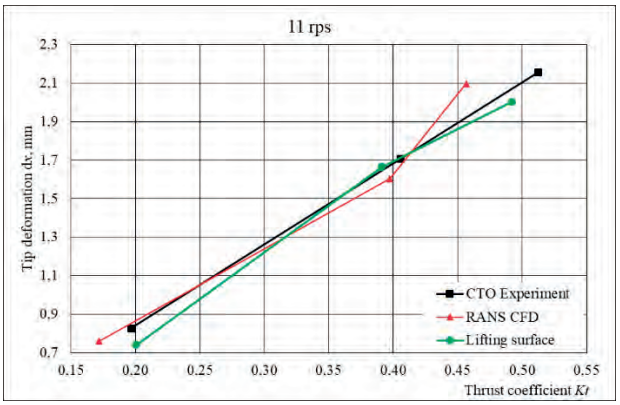

Fig. 24. Computed values for the tip deflection compared with experimental data, at 11 RPS

CONCLUSION AND FURTHER WORK

A comparison of the results obtained from the newly developed in-house tool shows that the proposed method, which involves combining a shell FEM model with the lifting surface model for flow simulation, is capable of correctly predicting the blade deformation, even for highly elastic materials under heavy load. The coupled tool remains quite effective; when used on a desktop PC with a 3.2 GHz CPU and with a mesh of 16 × 16 points like the one in the case presented here, the time required for the analysis of a single geometry variant and single loading condition was 15 min. Thus, if we assume that the analysis is run in a loop during the night, a designer can analyse approximately 60 variants of the propeller geometry in this time. However, the following limitations of the tool should be mentioned:

- The lifting surface flow model is not appropriate for the design of propellers that will operate primarily under bollard pull conditions (e.g. for tugs);
- A single layer of elements is a correct representation only for isotropic materials, and is also likely to be a sufficient approximation of some composites. However, it will not provide the required results for composites where the fibres are oriented to achieve coupling between bending and twisting. For such materials, several layers of elements are necessary.

The results obtained here indicate that the developed tool predicts the blade deformation correctly, with reasonable efficiency. Some small but noticeable differences were observed in the results, which may result both from the obvious limitations of potential flow model and from the uncertainties in the experiment, which is related to the following quantities:

- The setup of the angle of attack for the foil;
- The characteristics of the polymer material (test specimen vs. final product);
- The use of a camera with relatively low resolution for taking the pictures.

In the authors' opinion, the factors listed above and the standard uncertainty of the measuring devices (for load cells, flow speed etc.) mean that differences in the results of this order of magnitude cannot be avoided in this kind of comparison.

The limited content of the validation material and the abovementioned limitations of the tool itself suggest the following avenues for future work:

- Validation of our analyses for the case where strong coupling between blade deformation and hydrodynamic characteristics is observed, and verification of the correctness of the predicted trends.
- Extension of the FEM module to enable simulations for composite blades with coupled twisting and bending.
- Extension of the FEM module to enable the time-accurate FSI simulations, crucial from the point of view of the noise generation ([15], [16], [17]).
- Analysis of the propeller operation behind the ship hull with taking into account the rudder- propeller interaction, as presented in [18], at present, only the propeller in uniform flow was analysed.
- Studying the influence of the blade material (rigid vs. elastic) on the fouling, which also influences considerably the propeller performance [19].

ACKNOWLEDGEMENTS

The research was financed by the European Defence Agency, within the framework of the NextProp project (EDA CAT B project No B-1466-GEM1-GP).

REFERENCES

1. Mouritz A P, Gellert E, Burchill P, Challis K. Review of advanced composite structures for naval ships and submarines. *Composite Structures* 2001, 53(1):21–42, https://doi.org/10.1016/S0263-8223(00)00175-6.

2. Paul A, Schmidt A, Wolf E. Acoustically optimized propeller made from composite materials. *ThyssenKrupp Techforum* 2011, 1:58–63.

3. Pinninti R R, Raj S. Fabrication and analysis of composite marine propeller. *International Journal of Engineering Technology, Management and Applied Sciences* 2015, 3:238–45.

4. Suh S-B, Park I-R. Numerical simulation of the flow around the SUBOFF submarine model using a DES method. *Journal of the Society of Naval Architects of Korea* 2021, 58:73–83, https://doi.org/10.3744/SNAK.2021.58.2.073.

5. Lee H, Song M-C, Suh J-C, Chang B-J. Hydro-elastic analysis of marine propellers based on a BEM-FEM coupled FSI algorithm. *International Journal of Naval Architecture and Ocean Engineering* 2014, 6(3):562–577, https://doi.org/10.2478/IJNAOE-2013-0198.

6. Maung P T, Prusty B G, Phillips A W, St John N A. Curved fibre path optimisation for improved shape adaptive composite propeller blade design. *Composite Structures* 2021, 255:112961, https://doi.org/10.1016/j.compstruct.2020.112961.

7. Szantyr J A. A method for analysis of cavitating marine propellers in non-uniform flow. *International Shipbuilding Progress* 1994, 41(427):223–241, doi: 10.3233/ISP-1994-4142703.

8. Maljaars P, Kaminski M. Hydro-elastic analysis of flexible propellers: An overview. *Fourth International Symposium on Marine Propulsors* 2015, 146–58.

9. Y-B, Wang Z-K, G-C. Tsai G-C. Two-way fluid-structure interaction simulation of a micro horizontal axis wind turbine. *International Journal of Engineering and Technology Innovation* 2015, 5:33–44.

10. Langer U, Yang H. Numerical simulation of fluid–structure interaction problems with hyperelastic models: A monolithic approach. *Mathematics and Computers in Simulation* 2018, 145:186–208, doi: https://doi.org/10.1016/j.matcom.2016.07.008.

11. Young Y L. Fluid–structure interaction analysis of flexible composite marine propellers. *Journal of Fluids and Structures* 2008, 24(6):799–818, doi: https://doi.org/10.1016/j.jfluidstructs.2007.12.010.

12. Jarzyna H, Koronowicz T, Szantyr J. Design of marine propellers: Selected problems. Polish Academy of Science; 1994.

13. Szturomski B. Inżynierskie zastosowanie MES w problemach mechaniki ciała stałego na przykładzie programu ABAQUS [Engineering application of FEM in problems of solid mechanics on the example of the ABAQUS program - available in Polish]. Gdynia: Wydawnictwo Akademickie AMW; 2013.

14. Gokhale N, Deshpande S, Bedekar S, Thite A. Practical finite element analysis. Maharastra, India; 2008.

15. Guangnian L., Chen Q., Liu Y.. Experimental Study on Dynamic Structure of Propeller Tip Vortex. *Polish Maritime Research*, 2020;27(2): 11-18. https://doi.org/10.2478/pomr-2020-0022

16. Lou B., Cui H.. Fluid–Structure Interaction Vibration Experiments and Numerical Verification of a Real Marine Propeller, *Polish Maritime Research*, 2021;28(3): 61-75. https://doi.org/10.2478/pomr-2021-0034

17. Leshchev, V., Maslov, I., Palagin, O., Naydonov, A., Transfer function for a controllable pitch propeller with added water mass, *Polish Maritime Research* 4 (120) 2023 Vol. 30; pp. 74-80, 10.2478/pomr-2023-006

18. Quang P., Van Hung P., Cong N., Tung T.. Effects of Rudder and Blade Pitch on Hydrodynamic Performance of Marine Propeller Using CFD, *Polish Maritime Research*, 2022;29(2): 55-63. https://doi.org/10.2478/pomr-2022-0017

19. Zinati A., Ketabdari M., Zeraatgar H.. Effects of Propeller Fouling on the Hydrodynamic Performance of a Marine Propeller. *Polish Maritime Research* 2023;30(4): 61-73. https://doi.org/10.2478/pomr-2023-0059